26th AIAA Applied Aerodynamics Conference
18 - 21 August 2008, Honolulu, Hawaii

AIAA 2008-7062

Aerodynamic Fidelity of Sub-scale Two-Dimensional Ice Accretion Simulations

Greg Busch,[*] Andy Broeren,[†] and Michael Bragg[‡]
University of Illinois at Urbana-Champaign, Urbana, IL 61801

The objective of this study was to quantify the accuracy with which two-dimensional ice accretion simulations can be used on a ¼-scale airfoil model at low Reynolds number to simulate the aerodynamics of ice accreted on a full-scale airfoil model at high Reynolds number. Six full-scale ice accretion castings, representing ice roughness, streamwise ice, horn ice, and spanwise-ridge ice, were previously tested in the ONERA F1 wind tunnel at $Re = 12.0 \times 10^6$ and $M = 0.20$. These castings were digitized and measured to create sub-scale 2-D smooth and simple-geometry simulations, which were tested in the University of Illinois 3 x 4 ft. wind tunnel at $Re = 1.8 \times 10^6$ and $M = 0.18$. C_l, C_m, and C_d for each sub-scale simulation was compared with the corresponding full-scale casting. Geometrically-scaled simulations of the horn-ice and spanwise-ridge ice castings modeled $C_{l,max}$ to within 2% and $C_{d,min}$ to within 15%. Geometrically-scaled simulations of the ice roughness and streamwise ice tended to have conservative $C_{l,max}$ and C_d. The aerodynamic performance of simulations of these types of accretion was found to be sensitive to roughness height and concentration. Scaled roughness heights smaller than those found on the casting were necessary to improve simulation accuracy, resulting in $C_{l,max}$ and $C_{d,min}$ within 3% and 5% of the casting, respectively. Removing highly three-dimensional features, such as ice feathers, that became two-dimensional in the creation of 2-D smooth simulations was found to improve simulation aerodynamic fidelity.

Nomenclature

α	airfoil angle of attack
c	airfoil chord length
C_d	drag coefficient
$C_{d,min}$	minimum drag coefficient
$\Delta C_{d,rms}$	RMS difference in C_d between a simulation and casting over a range of angle of attack
C_l	lift coefficient
$C_{l,max}$	maximum lift coefficient
C_m	quarter-chord pitching-moment coefficient
C_p	pressure coefficient
k	feature height
L.S.	lower surface of airfoil
M	freestream Mach number
Re	freestream Reynolds number, based on the airfoil chord length
s	airfoil model coordinate along the surface length
θ	ice-shape horn or ridge angle with respect to the airfoil chordline
U.S.	upper surface of airfoil
x	coordinate in the airfoil model chordwise direction
y	coordinate normal to the airfoil model chordline
z	coordinate in the airfoil model spanwise direction

[*] Graduate Research Assistant, Department of Aerospace Engineering, Member AIAA.
[†] Research Scientist, Univ. of Illinois, Currently Aerospace Engineer, NASA Glenn Research Center, Associate Fellow AIAA.
[‡] Professor of Aerospace Engineering, Executive Associate Dean for Academic Affairs, Fellow AIAA.

I. Introduction

Determining the aerodynamic effects of ice accretion on aircraft surfaces is an important step in aircraft certification and ensuring safety. Ice accretion on the aircraft wing can cause significant reductions in maximum lift and substantial increases in drag. Quantifying these effects is frequently done either in flight testing or wind-tunnel testing. Flight testing is usually more complicated and expensive than wind-tunnel testing, as there is less predictability in the environment and the ice accretion geometry is not easily documented. Wind-tunnel testing is a less-expensive alternative to flight testing, but normally must be performed on sub-scale models to minimize tunnel blockage and reduce costs. Icing tunnels are used to generate ice accretions, but it is seldom possible to obtain high quality aerodynamic data directly from an accretion in an icing tunnel due to poor flow quality, icing cloud non-uniformity near the tunnel walls, and instrumentation difficulties. To measure the aerodynamic penalties associated with an accretion, it is usually necessary to simulate it in an aerodynamic wind tunnel. This study is part of a research program described by Bragg et al.[1] that seeks to address issues in sub-scale ice accretion simulation. The purpose of this study is to determine how well the aerodynamics of full-scale airfoils with ice accretion can be simulated using simplified simulations on a sub-scale model.

Several different types of simulations have been used to model ice accretion aerodynamics. The highest fidelity type of simulation is a casting of the original ice accretion. Castings model nearly every feature of the accretion, from small-scale surface roughness to large-scale spanwise variation. Unfortunately, castings are expensive to produce and require time in an icing wind tunnel. Additionally, at this time, castings can not be scaled, so the icing model used to obtain a casting must be the same or similar scale as the aerodynamic model. These constraints make it advantageous to use simplified simulations instead of castings to model the aerodynamics of the accretion. Therefore, sub-scale simulation techniques need to be validated for use on aerodynamic models.

Two of the most common sub-scale simulation types are 2-D smooth simulations and simple-geometry simulations. A 2-D smooth simulation is a constant-cross section extrusion of a tracing of the ice accretion. The tracing usually needs to undergo a smoothing process to make it suitable for extruding, and the NASA Glenn developed software SmaggIce[2] is frequently implemented for this smoothing. A simple-geometry simulation uses extruded geometric shapes, such as rectangles and quarter rounds, to represent an ice accretion. Simple-geometry simulations are normally two-dimensional, and are considered to be of lower fidelity than 2-D smooth simulations. The low cost and minimal fabrication effort of simple-geometry simulations makes them ideal for use in parametric studies, such as that of Papadakis et al.[3] and Kim.[4] Frequently, surface roughness is added to the two-dimensional simulations to make them more representative of the ice accretion.

Bragg, Broeren, and Blumenthal[5] have investigated the main aerodynamic characteristics of ice accretions and created four categories of ice accretion: ice roughness, streamwise ice, horn ice, and spanwise-ridge ice. Ice roughness refers to the initial build-up of ice before a larger accretion forms. The roughness extracts energy from the boundary layer, causing premature trailing-edge separation and a resulting trailing-edge stall. Streamwise ice usually forms in conditions well-below freezing and conforms to the airfoil leading edge. The slope discontinuity at the ice-airfoil interface sometimes causes a laminar separation bubble to form. Downstream of the stagnation line are regions of highly three-dimensional feathers which extract momentum from the airfoil boundary layer and cause premature flow separation, similar to ice roughness. Horn ice usually forms at temperatures just below freezing, as impinging droplets do not freeze immediately upon impact but instead flow for a short time along the airfoil surface and then freeze, forming nodules which coalesce into an ice horn. The severe adverse pressure gradient at the tip of the horn generates a separation bubble, similar to the laminar long bubble described by Tani.[6] This separation bubble dominates the airfoil aerodynamics and induces a thin-airfoil stall, as characterized by McCullough and Gault.[7] The main geometric parameters affecting separation bubble size are horn height (k/c), angle (θ), location (s/c), and sometimes tip radius (r/c), depending on the airfoil. Spanwise-ridge ice often results from supercooled large droplet (SLD) conditions or from the use of a thermal ice protection system (IPS) that is operating at less than 100% evaporation, which allows water droplets to flow back to the unprotected portion of the airfoil and freeze, forming a ridge. As with horn-ice, a separation bubble usually forms downstream of a spanwise-ridge ice accretion. However, the flowfield is qualitatively different from that of a horn-ice accretion because the boundary layer has time to develop before reaching the accretion.

In a previous study at the University of Illinois,[8,9,10] several different simulation types were built for a sub-scale, 18-inch chord NACA 23012 aerodynamic model to emulate ice accreted on a sub-scale, 18-inch chord NACA 23012 icing model. For that study, the icing conditions were selected to produce ice accretions with gross geometry similar to that which would form on a full-scale airfoil. 2-D smooth simulations (some with additional surface roughness), carefully constructed from tracings representative of the average ice accretion geometry, modeled $C_{l,max}$

to within 2% for all accretion types. Simple-geometry simulations yielded similar comparisons. The angle of attack at which $C_{l,max}$ occurred was accurately captured to within 1 deg. for all accretion types except the spanwise-ridge ice, for which the 2-D smooth simulation stalled 2 deg. earlier than did the corresponding casting. C_d was accurately modeled for the ice roughness, streamwise-ice, and horn-ice simulations (again, with the proper addition of surface roughness). However, significant spanwise variation in the flowfield of the 2-D smooth spanwise-ridge ice simulation made it difficult to determine its ability to accurately model C_d of the casting in this study. These results show that by accurately capturing the gross accretion geometry, ice accretion aerodynamics at equivalent geometric scale, Reynolds number, and Mach number may be accurately modeled using simplified, two-dimensional simulations.

The effects of Reynolds and Mach number on ice accretion aerodynamics have been documented in several studies. Broeren et al.[11] found that $C_{l,max}$ changed very little over a Reynolds number range of $4.6 \times 10^6 - 16 \times 10^6$ and a Mach number range of 0.10 – 0.28 for most types of ice accretion on a NACA 23012 airfoil. Addy and Chung[12] obtained similar results over a similar Reynolds number range for a 36-inch chord NLF-0414 airfoil. Papadakis et al.[13] varied Reynolds number from $2 \times 10^6 - 4 \times 10^6$ and from $0.5 \times 10^6 - 2.0 \times 10^6$ on 57-inch chord and 24-inch chord modified NACA 63_A213 airfoil models, respectively. No notable Reynolds number effects were observed on the larger model, but $C_{l,max}$ decreased by about 9% as Reynolds number was increased on the smaller model. The dependence on Reynolds number in this range may be airfoil and ice shape dependent, as Lee et al.[14] report very little effect of Reynolds number over a range of $0.5 \times 10^6 - 1.8 \times 10^6$ on $C_{l,max}$ of a NACA 23012m with a spanwise-ridge ice accretion. Regardless, the Reynolds number range of interest in the current study is $1.8 \times 10^6 - 12 \times 10^6$, where Reynolds number effects have been shown to be small.

Papadakis et al.[13] used airfoil models of different chords to investigate the effects of geometric scaling on the aerodynamic penalties caused by 2-D smooth and simple-geometry horn-ice simulations. Geometrically scaled ice simulations on 57-inch chord and 24-inch chord models at identical Reynolds number yielded similar penalties to $C_{l,max}$, suggesting that geometric scaling may be appropriate for these low fidelity horn-ice simulations, at least for the modified NACA 63_A213 on which the test was conducted. That study, and the studies summarized above, compared sub-scale ice simulations with either sub-scale ice accretion castings at similar Reynolds number, sub-scale ice accretion castings at high Reynolds number, or full-scale ice simulations at similar Reynolds number, or they looked at Reynolds and Mach number effects on ice accretion castings and simulations. The current study compares sub-scale ice simulations at low Reynolds number to full-scale ice accretion castings at high Reynolds number.

The objective of this study is to quantify the accuracy with which 2-D smooth and simple-geometry simulations can be used on a ¼-scale airfoil model to simulate the aerodynamics of ice accreted on a full-scale airfoil model at a higher *Re*. Sub-scale simple-geometry and 2-D smooth simulations of six full-scale ice accretions were constructed. The aerodynamic penalties due to each of these simulations were measured in the University of Illinois 3 x 4 ft. subsonic wind tunnel at $Re = 1.8 \times 10^6$ and $M = 0.18$ and compared with the penalties caused by the full-scale castings at $Re = 12.0 \times 10^6$ and $M = 0.20$.

II. Experimental Methods

All sub-scale aerodynamic testing was conducted in the University of Illinois subsonic, low-turbulence, open-return wind tunnel, which had a test section measuring 2.8 ft. high, 4 ft. wide, and 8 ft. long. The test section widened approximately 0.5 inches over its length to account for growth in the wall boundary layer. The inlet contraction ratio of the tunnel was 7.5:1. A four-inch honeycomb and four anti-turbulence screens were used to reduce the empty test-section turbulence intensity to less than 0.1% at all operating speeds over a frequency range of 10-5000 Hz.[15]

The aluminum NACA 23012 airfoil model used in this study had a chord of 18 inches and a span of 33.563 inches. A removable leading edge facilitated simple installation of ice accretion simulations. The airfoil model had two chordwise rows of taps: a primary row of 43 taps located at 51% span and a secondary row of 22 taps located at 42% span. Additionally, the model had a row of spanwise taps on the upper surface, located at 70% chord. The layout of these taps made it possible to check for spanwise variation in the flow behind the ice shapes. The airfoil model is described in more detail by Blumenthal.[16]

Lift and pitching moment coefficient data were obtained using both a three-component force balance and by integrating the measured surface pressures around the airfoil model. The drag coefficient was computed using data collected by a traversable wake rake which measured the static and total wake pressures using 25 probes. This wake rake is shown installed behind the airfoil model in Fig. 1. All drag measurements reported in this paper were taken with the wake rake at a spanwise station 4.13 inches above the model centerline. An electronically scanned pressure system was used to measure the model surface and wake pressures. The pressures measured by the wake rake were

used to obtain the drag coefficient using standard momentum-deficit methods. Blumenthal[16] describes the experimental setup in more detail. All testing reported in this paper was conducted at Re = 1.8 x 10^6 and M = 0.18.

Fluorescent oil-flow visualization images were also taken of the spanwise-ridge ice simulations for comparison with the full-scale casting. For these images, the airfoil model was coated with fluorescent oil that was subject to surface shear stresses. Regions of high shear stress caused more oil movement than regions of low shear stress, so these regions do not appear to be as bright as the low shear stress regions. Using this technique, the flowfield can be examined to identify separation bubble reattachment zones as well as regions of separation and reverse flow.

Ice accretion castings were acquired in the NASA Glenn Icing Research Tunnel on a 72-inch chord NACA 23012 airfoil model for six different ice accretions: glaze ice roughness, rime ice roughness, two streamwise-ice accretions, a horn-ice accretion, and a spanwise-ridge ice accretion (Fig. 2). The conditions and details of this test are explained in more detail by Bragg et al.[1] The aerodynamic penalties associated with these castings were measured in the ONERA F1 wind tunnel, also on a 72-inch chord NACA 23012 airfoil model, and are discussed in detail by Broeren et al.[11] These data are considered to give the true aerodynamic performance associated with each type of accretion and are used as the baseline for comparison in the current study.

Fig. 1 Wake rake installed behind NACA 23012 airfoil model.

Each ice accretion was simulated on a ¼-scale, 18-inch chord NACA 23012 airfoil model. Sub-scale simple-geometry simulations were used to model the ice roughness accretions by adding grit roughness in the appropriate chordwise locations. The other accretion types were modeled using 2-D smooth simulations, constructed using rapid-prototyping techniques, and simple-geometry simulations, constructed using simple, off-the-shelf materials. The 2-D smooth simulations were extruded from the tracings of the castings shown in Fig. 2 and pressure taps were installed. Each 2-D smooth simulation was formed by three duplicate 11.187-inch long sections placed end-to-end to cover the span of the airfoil model.

The simple-geometry simulations were not pressure tapped, so all lift and pitching moment comparisons involving these simulations are based on force-balance data. Grit roughness of various sizes was added to many of the 2-D smooth and simple-geometry simulations to model the roughness of the ice accretion. The aerodynamic penalty associated with each of these sub-scale simulations was compared to that of the corresponding full-scale casting to quantify the aerodynamic fidelity of the simulation.

III. Results and Discussion

In the following sections, comparisons are made between aerodynamic performance data for a sub-scale 18-inch chord NACA 23012 airfoil at Re = 1.8 x 10^6 and a full-scale 72-inch chord NACA 23012 airfoil at Re = 12.0 x 10^6, both for the clean case and with ice accretion simulations installed. High fidelity, cast ice simulations were used on the full-scale model and are compared with simple-geometry and 2-D smooth ice simulations used on the sub-scale model. Broeren et al.[11] discuss in detail the effects of the ice castings on the full-scale NACA 23012 performance at Re = 12.0 x 10^6, so these effects will not be discussed here. Instead, the present discussion will focus on comparisons between the simplified, sub-scale simulations and the full-scale ice castings. For completeness, the clean airfoil performance will be summarized first.

Clean NACA 23012

The effects of Reynolds number on the aerodynamic performance of a clean NACA 23012 airfoil are substantial. Figure 3 shows C_l, C_m, and C_d measured for two Reynolds numbers, Re = 12.0 x 10^6 and Re = 1.8 x 10^6, for approximately equal Mach numbers. Leading-edge stall is exhibited at both Reynolds numbers, but occurs at α = 14.4 deg. at the lower Reynolds number, approximately 3.7 deg. lower than at the higher Reynolds number. Also at the lower Reynolds number, the NACA 23012 has a shallower lift-curve slope and a $C_{l,max}$ of 1.48, 20% lower

than at the higher Reynolds number. The dependence of pitching moment on angle of attack was greater for the lower Reynolds number case, and became nose-up at a much lower angle of attack. Finally, the C_d curve at the lower Reynolds number was narrower than at Re = 12.0 x 10^6, was shifted upwards (resulting in a $C_{d,\alpha=0}$ = 0.0068), and demonstrated a more pronounced low-drag region from approximately 0 to 6 deg. than did the higher Reynolds number case. These clean airfoil data have been validated by comparison to other measurements of NACA 23012 airfoil performance,[11] and the trends are typical for conventional airfoils. As discussed in the Introduction (and shown later in this paper), many of these effects disappear or are mostly mitigated when ice accretes.

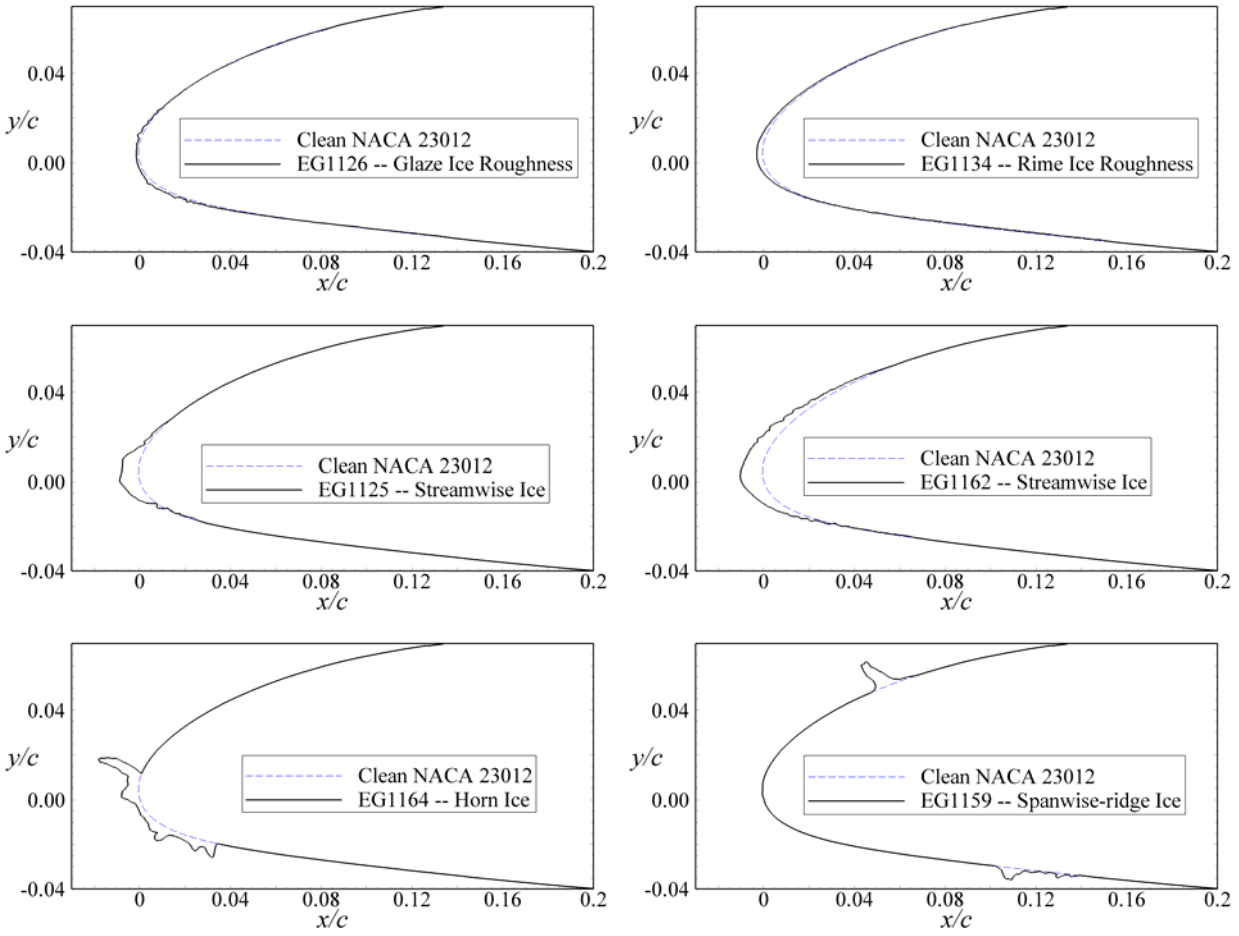

Fig. 2 Tracings of each of the six ice accretion castings simulated in this study. The tracings of the streamwise ice, horn ice, and spanwise-ridge ice accretions were extruded to form 2-D smooth simulations.

Ice Roughness Simulations

Two types of ice roughness were simulated in this study: glaze-ice roughness and rime-ice roughness (Fig. 2). On the airfoil upper surface, the glaze-ice roughness extended from x/c = 0.000, where it had a height k/c = 0.0016. The roughness height tended to diminish gradually until x/c = 0.026, where the roughness ended. Similarly, the glaze-ice roughness on the airfoil lower surface extended from x/c = 0.004, where it had a height k/c = 0.0011. Again, the height tended to diminish gradually until the roughness ended at x/c = 0.041. The rime-ice roughness had a much longer chordwise extent, from x/c = -.002 to 0.080 on the upper surface and from approximately x/c = 0.000 to 0.200 on the lower surface. The maximum height was about k/c = 0.0003 on each surface, occurring near the most upstream chordwise extent, with the roughness height diminishing to zero at the most rearward extent. The stagnation line on both the glaze and rime-ice accretions was relatively smooth and free of roughness.

The effects of the glaze-ice roughness on C_l, C_m, and C_d of the NACA 23012 are shown in Fig. 4. Again, the data for the full-scale casting was acquired at Re = 12.0 x 10^6 and M = 0.20, and the data for all other simulations was acquired at Re = 1.8 x 10^6 and M = 0.18. The addition of the full-scale casting caused the airfoil to achieve a $C_{l,max}$ of only 1.08 and to stall at approximately 11.8 deg. It also caused a more nose-up pitching moment at high

angles of attack and increased C_d to 0.0096 at $\alpha = 0$ deg. Several simple-geometry simulations were constructed by adding various roughness sizes to the NACA 23012 airfoil over the appropriate chordwise extent to duplicate the aerodynamic effects of the casting. The first simulation used several different roughness sizes on the upper and lower surface, chosen to match the k/c of the roughness on the casting at several chordwise stations. Roughness strips with heights k/c = 0.0013, 0.0006, 0.0009, and 0.0005, were placed on the airfoil upper surface to match the chordwise extent of the casting roughness. Roughness strips of height k/c = 0.0009, 0.0007, 0.0009, and 0.0003 were placed on the lower surface, again to match the roughness extents on the casting. Figure 4 shows that this caused too large of an aerodynamic penalty, resulting in a $C_{l,max}$ 3.9% too low and a C_d too high at low angles of attack. Therefore, other simulations were used to more closely match the aerodynamic performance of the casting. The simulation which most accurately modeled $C_{l,max}$ used roughness with a height k/c = 0.0003, and had a $C_{l,max}$ only 0.6% below that of the casting. This simulation modeled C_d more accurately at low angles of attack, but tended to have a lower C_d at angles of attack beyond $\alpha = 4$ deg.

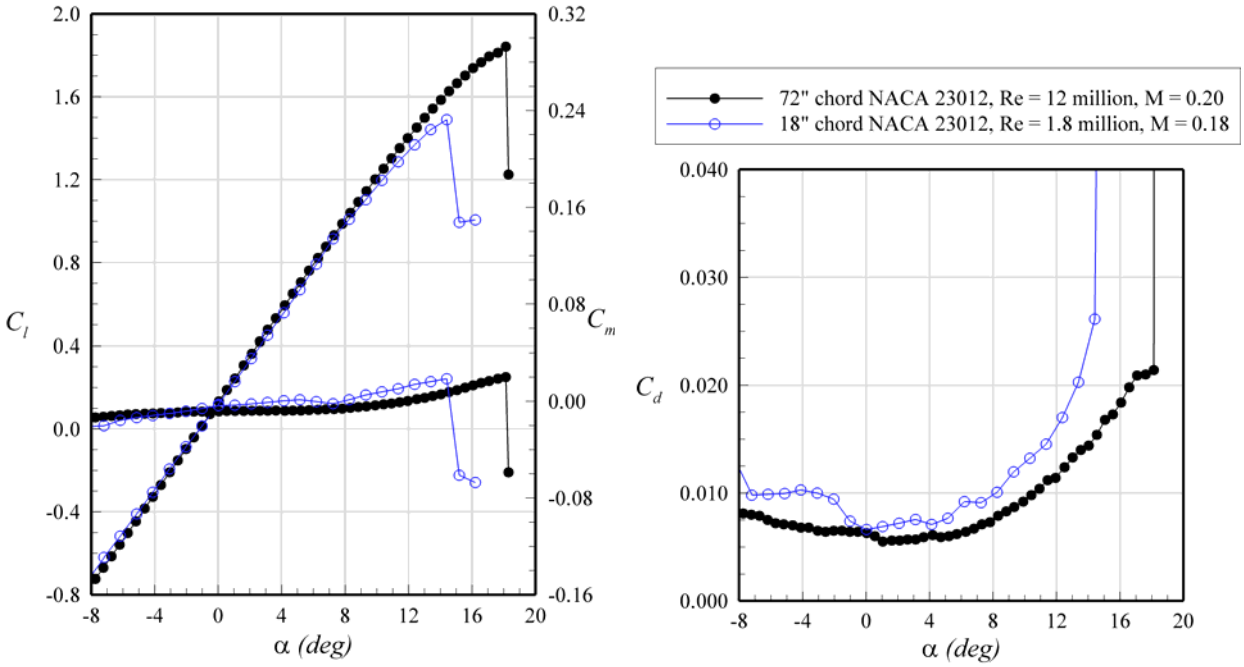

Fig. 3 Comparison of full-scale and sub-scale clean NACA 23012 performance.

A third simulation was designed to represent only the initial portion of roughness on the casting. For this simulation, roughness strips of width s/c = 0.0056 were placed on the clean airfoil at a location corresponding to the most upstream extent of the roughness on the casting. The heights of this roughness matched the maximum height of roughness on the casting, k/c = 0.0013 and k/c = 0.0009 on the upper and lower surfaces, respectively. This resulted in $C_{l,max}$ nearly identical to the first simulation discussed, which matched k/c of the casting over the entire chord. These results suggest that, for the NACA 23012 airfoil, $C_{l,max}$ is not sensitive to the chordwise extents of roughness, at least if the most upstream roughness is larger than roughness located farther downstream. This third simulation modeled C_d of the casting at low angle of attack slightly more accurately than did the other simulations, but like the k/c = 0.0003 roughness simulation, had a lower C_d at angles of attack above $\alpha = 4$ deg. This further suggests that C_d is sensitive to both roughness size and chordwise extent.

A useful metric for comparing C_d at multiple angles of attack is the percent RMS difference in C_d over an appropriate angle of attack range. The angle of attack range used in this study was that over which C_l varied linearly with α. The value $\Delta C_{d,rms}$ is a percentage and is computed by determining the RMS of the percent difference between the casting C_d and simulation C_d at each angle of attack in the linear range (a total of N angles of attack):

$$\Delta C_{d,RMS} = \sqrt{\frac{\sum_{i=1}^{N}\left(\frac{C_{d,sim}^{i} - C_{d,casting}^{i}}{C_{d,casting}^{i}} x100\%\right)^{2}}{N}} \quad (1)$$

The first simulation discussed, which varied roughness height along the chord to match *k/c* of the roughness on the casting, had a $\Delta C_{d,rms}$ = 20.3% over a range of angle of attack from α = -4 to 9 deg. This was improved to 11.4% for the simulation which modeled only the first *s/c* = 0.0056 of the roughness on the casting (Fig. 4).

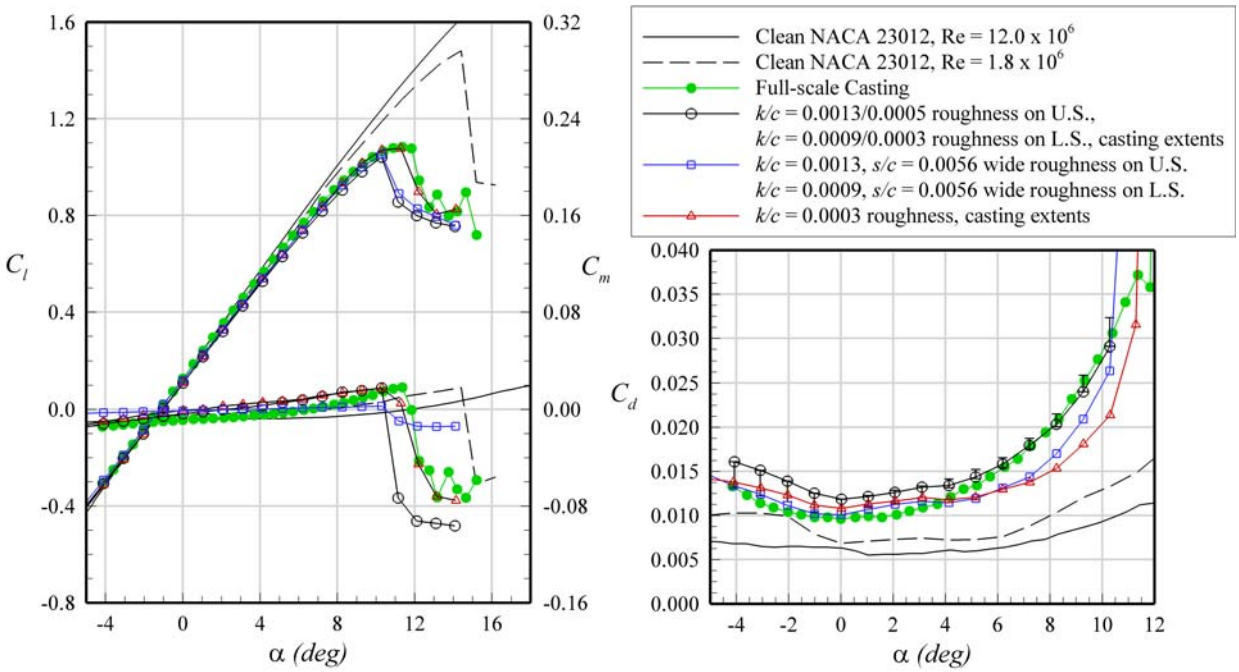

Fig. 4 Comparison of C_l, C_m, and C_d of EG1126 glaze ice roughness simulations. The casting data were acquired at *Re* = 12.0 x 10^6 and *M* = 0.20, all other ice simulation data were acquired at *Re* = 1.8 x 10^6 and *M* = 0.18. The error bars indicate the variation in C_d along the airfoil span.

An important factor to consider when comparing values of C_d is the method by which C_d is measured. It is common for C_d to vary along the span of an iced airfoil, but the full-scale casting C_d data presented in this paper were taken at only a single spanwise station. Most of the sub-scale data presented were also taken at a single spanwise station, although these data were all acquired in the same facility at identical spanwise stations. To give an estimate for the magnitude of the variation in C_d on the sub-scale model, measurements of C_d at five spanwise stations located two inches apart were taken for selected cases. The maximum and minimum values of C_d measured during this spanwise sweep are indicated with error bars in Fig. 4 (based on the *k/c* = 0.0013/0.0005 U.S., *k/c* = 0.0009/0.0003 roughness simulation). This variation in C_d was greatest at angles of attack below α = 0 deg., on the order of 17%. At higher angles of attack, the variation was around 8%; similar results were obtained in previous studies on iced airfoils.[16,17] It is likely that the C_d of the casting had similar spanwise variations. The level of agreement of C_d between the casting and simulations is therefore dependent on the spanwise station at which C_d is measured, and it is recommended that in future testing, when possible, C_d be measured at several spanwise stations and averaged for comparison. For the simulations tested in this study, useful C_d comparisons can still be obtained. In Fig. 4, for example, C_d of the *k/c* = 0.0003 simulation was clearly lower than the casting C_d at angles of attack above α = 6 deg., even with consideration of spanwise variation in C_d.

The mismatch in aerodynamic performance between the casting and the simple-geometry simulation with matched *k/c* values prompted an investigation into the effect of roughness concentration. In this paper, roughness concentration is defined as the percentage of airfoil surface area covered by individual roughness elements over the relevant chordwise extents. It has been shown in past studies[8,18] that roughness concentration may have an

important effect on $C_{l,max}$, especially at low concentrations. Figure 5(a) shows the effect of increasing roughness concentration on $C_{l,max}$ of the NACA 23012 airfoil at Re = 1.8 x 10^6 (for a roughness height of k/c = 0.0018). As roughness concentration increases, $C_{l,max}$ decreases, up to a concentration of about 20% in this case. Beyond this concentration, $C_{l,max}$ is relatively insensitive to changes in roughness concentration. These results are consistent with those of earlier studies. [8,18] Interpolating from Fig. 5, the simple-geometry simulation with a $C_{l,max}$ most similar to that of the casting has a roughness concentration of 8%.

A comparison of C_d between the casting and each sub-scale simulation is given in Fig. 5(b). In this figure, a value of $\Delta C_{d,rms}$ = 0 corresponds to perfect agreement between the casting and simulation, so smaller values of $\Delta C_{d,rms}$ indicate better agreement with C_d of the casting. The horizontal dashed line shows $\Delta C_{d,rms}$ for the clean NACA 23012 airfoil; this indicates how well the clean airfoil simulates C_d of the casting. For a roughness height of k/c = 0.0018, a concentration of 7% yielded the best agreement with the casting C_d while also having a similar $C_{l,max}$. Note that beyond a concentration of 20%, $\Delta C_{d,rms}$ continues to change, suggesting that C_d does not remain as constant as $C_{l,max}$ for concentration variations in this range.

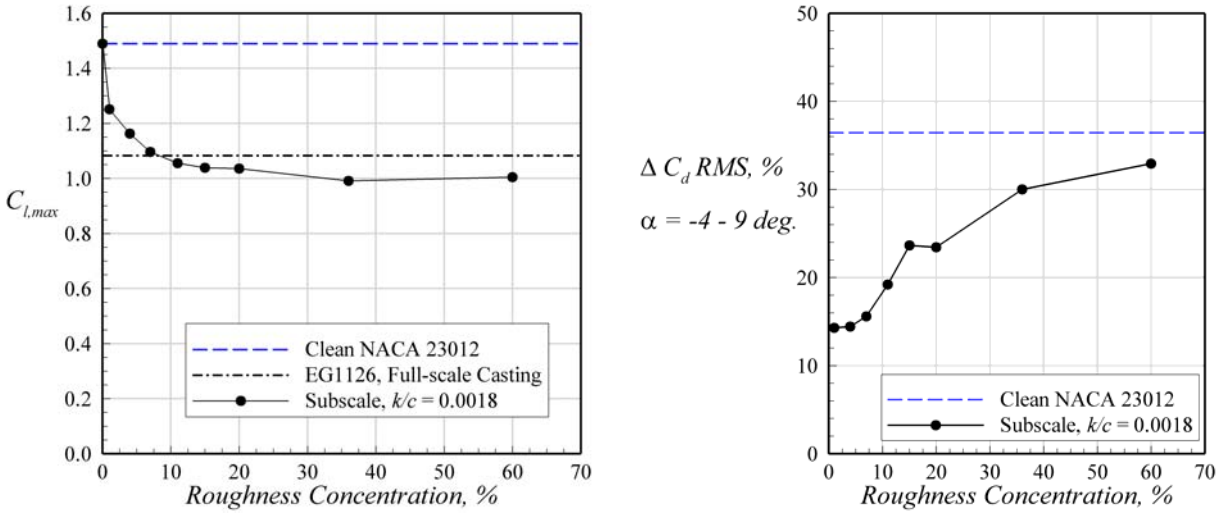

(a) **(b)**

Fig. 5 Effect of simulated roughness concentration on comparisons of (a) $C_{l,max}$ and (b) C_d with the full-scale casting on the NACA 23012 airfoil. The roughness chordwise extents are those of the EG1126 casting: x/c = 0.000 to 0.026 on the upper surface and x/c = 0.004 to 0.041 on the lower surface.

The actual roughness concentration on the casting varied continuously along the chord and could not be accurately measured in this study. For most of the sub-scale simulations presented here, roughness was applied in a sufficiently high concentration to saturate the double-sided tape used to bond the roughness to the airfoil model. This concentration is referred to as the maximum concentration and varies with roughness size. Maximum concentration is about 60% for k/c = 0.0018 roughness and 85% for k/c = 0.0003 roughness. For most simulations, maximum roughness concentration was applied in order to mitigate roughness concentration effects.

The high degree of dependence of aerodynamic performance on roughness height motivated further investigation of this parameter. Several different simple-geometry simulations were built in addition to those described above by attaching roughness of various heights to the sub-scale airfoil over the same chordwise extents as the EG1126 casting (x/c = 0.000 – 0.026 on the upper surface, x/c = 0.004 – 0.041 on the lower surface). For each of these simulations, roughness was applied in maximum concentration. Figure 6(a) shows $C_{l,max}$ of each of these simulations compared to the clean NACA 23012 airfoil at Re = 1.8 x 10^6 and the full-scale casting at Re = 12.0 x 10^6.

The maximum roughness height and $C_{l,max}$ of the EG1126 casting are indicated. Not surprisingly, for the sub-scale simulations, $C_{l,max}$ decreases as roughness height increases. It is interesting to note that for small roughness heights, this change in $C_{l,max}$ is very rapid, but for roughness heights greater than k/c = 0.0003, the dependence of $C_{l,max}$ on k/c decreases. In Fig. 6, the roughness height for which the $C_{l,max}$ of the simulation is the same as that of the casting is about k/c = 0.0003, corresponding to the intersection of the line representing $C_{l,max}$ of the full-scale casting with the curve representing $C_{l,max}$ for various simulations. Figure 6(b) shows comparisons in C_d between the full-scale casting and each simulation of different roughness size. Adding roughness sizes below k/c = 0.0005

yielded the closest C_d to the casting, with $\Delta C_{d,rms} \approx 16\%$. A roughness size of $k/c = 0.0003$ at maximum concentration had values of both $C_{l,max}$ and C_d in reasonably good agreement with the casting; this is one of the cases for which data are shown in Fig. 4.

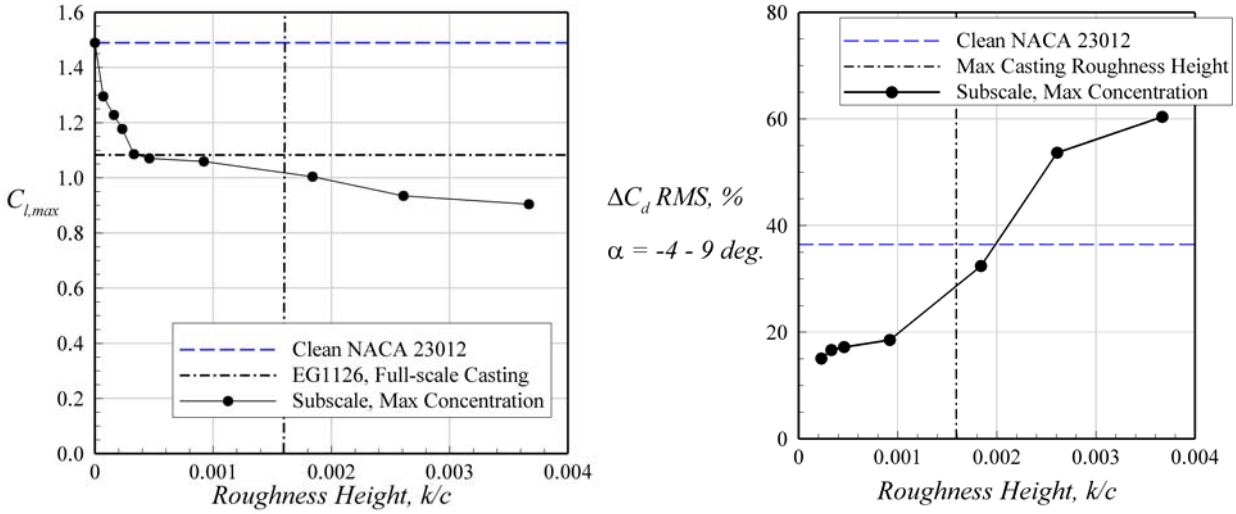

Fig. 6 Effect of simulated roughness height on comparisons of (a) $C_{l,max}$ and (b) C_d with the full-scale casting on the NACA 23012 airfoil. The roughness chordwise extents are those of the EG1126 casting for roughness heights above $k/c = 0.002$ and of the EG1134 casting for smaller roughness heights.

From these plots, it is clear that multiple simple-geometry simulations using different combinations of roughness height and concentration may have the same $C_{l,max}$ as the casting. The effect of surface roughness is to reduce boundary-layer momentum, causing it to thicken and separate earlier than it would in the absence of roughness.[5] It seems reasonable that a lower concentration of larger roughness elements could extract a similar amount of momentum as a higher concentration of smaller roughness elements. The key to modeling the degradation in $C_{l,max}$ due to ice roughness therefore is to select a combination of roughness height and concentration such that the simple-geometry simulation extracts the proper amount of momentum from the boundary layer. Since both roughness height and concentration continuously vary with chordwise position on the ice accretion, it is not clear how to define this height/concentration combination. While it is difficult to accurately measure roughness concentration on an ice casting, height can more easily be measured. However, roughness height measurements need to be based on the clean airfoil surface below the ice, which often is not accessible in regions of high roughness concentration, so these measurements have a large degree of uncertainty. In this study, emphasis is placed on roughness height, and a sufficiently large roughness concentration is used so that the simulation is in the range of Fig. 5(a) where $C_{l,max}$ is relatively insensitive to concentration. Using this approach, roughness concentration effects can be minimized.

The effect of the EG1134 rime-ice roughness casting, described at the beginning of this section, on airfoil performance is shown in Fig. 7. The degradation in $C_{l,max}$ was not as severe as it was for the glaze-ice roughness, with the casting reaching a value of 1.28, and stall occurring at a slightly higher angle of attack of 12.9 deg. The C_d curve was shifted upwards by about the same amount as with the glaze-ice roughness, with $C_{d,\alpha=0} = 0.0095$, but C_d is much lower at high angle of attack for the rime-ice roughness. The roughness height on the EG1134 casting was $k/c = 0.0003$ near the leading edge. As with the glaze-ice roughness simulations, simulated rime-ice roughness with approximately the same k/c as that of the casting (approximately $k/c = 0.00033$) was found to cause an aerodynamic penalty larger than that caused by the casting, resulting in $C_{l,max}$ 15.7% too low. Over a narrow range of angle of attack, from $\alpha = 4$ to 6 deg., C_d of the $k/c = 0.00033$ roughness simulation agreed very well with the casting. However, at all other angles of attack, C_d was much too high, giving $\Delta C_{d,rms} = 29.5\%$ from $\alpha = -4$ to 10 deg. Note that this $k/c = 0.00033$ roughness simulation had chordwise extents matching those of the EG1126 glaze-ice casting rather than the EG1134 rime-ice casting. The $k/c = 0.00033$ roughness simulation had already been tested for the glaze-ice roughness case, and increasing the roughness extents to those on the EG1134 casting would have little effect on $C_{l,max}$ (as discussed earlier) and would cause C_d to increase slightly. C_d was already too high for this simulation, so changing the roughness extents would not have improved the simulation fidelity.

For the high roughness concentrations used in this study, the most accurate simple-geometry simulation consisted of k/c = 0.00007 roughness. This simulation had a $C_{l,max}$ within 1% of the casting at a similar angle of attack, and the C_d curves were very similar up to α = 12 deg., as shown. The percent RMS difference in C_d between the casting and the k/c = 0.00007 roughness simulation was 6.8%, computed using Eq. (1) for α = -4 to 10 deg. The results for a simulation consisting of k/c = 0.00016 roughness is also shown in Fig. 7 to show the high sensitivity of $C_{l,max}$ and C_d to small changes in roughness height for roughness heights in this range.

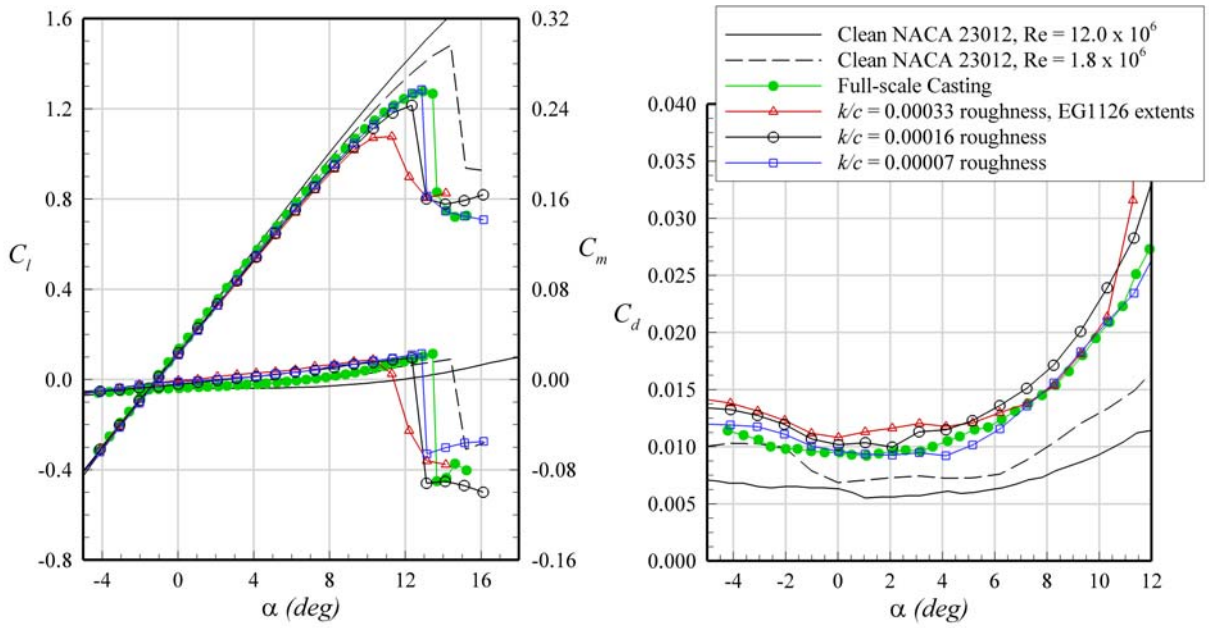

Fig. 7 Comparison of C_l, C_m, and C_d of EG1134 rime ice roughness simulations.

Streamwise-ice Simulations

Two types of streamwise-ice accretion were simulated in this study, one with a surface-slope discontinuity near the leading edge of the airfoil (EG1125) and a second with a geometry that was more conformal to the airfoil leading edge (EG1162). Figure 2 shows tracings of each of these accretions. The first streamwise-ice accretion, EG1125, had a combination of roughness and feathers extending from x/c = -0.008 to 0.019 on the upper surface of the airfoil and from x/c = -0.006 to 0.029 on the lower surface. As with the ice roughness accretion discussed earlier, on both the upper and lower surfaces the roughness height and concentration gradually decreased from a maximum value at the most upstream extent to zero at the most downstream extent. The maximum roughness height of the EG1125 accretion was approximately k/c = 0.0018 on the upper surface and k/c = 0.0012 on the lower surface. The more conformal streamwise accretion, EG1162, had a combination of surface roughness and ice feathers extending from x/c = -0.008 to 0.065 on the upper surface and from x/c = -0.005 to 0.060 on the lower surface. The maximum roughness heights on this accretion were k/c = 0.0014 and k/c = 0.0011 on the upper and lower surfaces, respectively. Extents corresponding to those on the appropriate casting were used when grit roughness was applied to the sub-scale simulations.

The aerodynamic performance coefficients C_l, C_m, and C_d are shown in Fig. 8 for the simulations of the EG1125 streamwise-ice accretion. As with the ice roughness case described above, the full-scale casting and clean NACA 23012 data were taken in the F1 wind tunnel at a Re = 12.0 x 10^6 and M = 0.20 while the sub-scale simulation data were taken in the University of Illinois wind tunnel at Re = 1.8 x 10^6 and M = 0.18. Again, the full-scale casting is considered to give the true aerodynamic performance coefficients of the ice accretion at flight Reynolds number. The casting caused the airfoil to stall at α = 11.9 deg., reducing $C_{l,max}$ to 1.12. Additionally, it changed the stall characteristics to a much more gradual, trailing-edge type stall. This effect is similar to that caused by the addition of ice roughness. C_d was increased by the addition of the casting, with $C_{d,min}$ = 0.0082 occurring at α = 1.6 deg. This is 47% higher than $C_{d,min}$ of the NACA 23012 airfoil at Re = 12.0 x 10^6, but only 24% higher than $C_{d,min}$ of the NACA 23012 airfoil at Re = 1.8 x 10^6. $C_{d,min}$ occurs at different angles of attack for each case.

In Fig. 8, four sub-scale simulations are compared with the full-scale casting. The 2-D smooth simulation is a rapid-prototyped constant cross-section representation of the accretion, with no roughness added. The simple

geometry simulation is a constant cross-section simulation built from off-the-shelf materials to capture the main geometric features of the accretion (Fig. 9). The 2-D smooth simulation with added roughness represents the simulation that would have been designed *without* a priori knowledge of the casting aerodynamics; the roughness has approximately the same non-dimensional height (*k/c*) as the roughness on the casting. The 2-D smooth simulation covered with tape was the simulation with the most similar aerodynamic performance to the casting, and was designed *with* a priori knowledge of the casting aerodynamics.

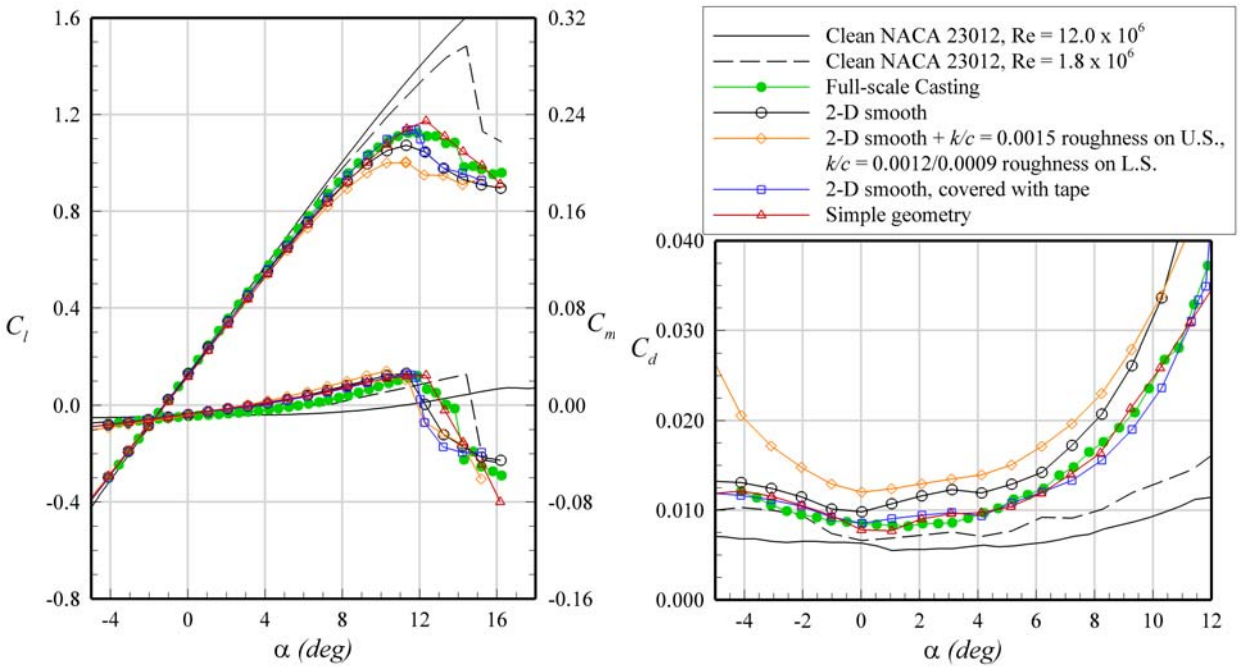

Fig. 8 Comparison of C_l, C_m, and C_d of EG1125 streamwise-ice simulations. The casting data were acquired at Re = 12.0 x 10^6 and M = 0.20, all other ice simulation data were acquired at Re = 1.8 x 10^6 and M = 0.18.

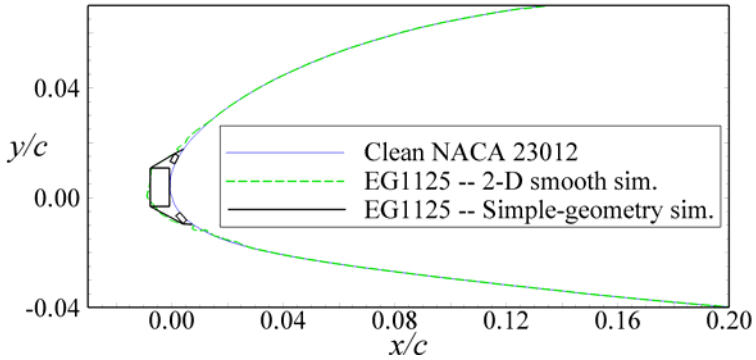

Fig. 9 Comparison of cross-section of EG1125 streamwise ice 2-D smooth and simple-geometry simulations.

At Re = 1.8 x 10^6, the 2-D smooth simulations with and without roughness caused a larger penalty to both $C_{l,max}$ and C_d than the casting, but caused a similar stall behavior. For the 2-D smooth simulation without roughness, $C_{l,max}$ was 6% lower than the casting and occurred at a 0.6 deg lower angle of attack, while $C_{d,min}$ was higher than that of the casting by about 19%. Adding roughness of the same *k/c* as the casting caused $C_{l,max}$ to decrease a further 6% relative to the casting and $C_{d,min}$ to increase a further 26%. At high angles of attack, C_d of the two simulations converged, suggesting that roughness plays a smaller role near stall than at low angles of attack.

In contrast to these two simulations, the simple-geometry simulation had a $C_{l,max}$ that was 4.4% higher than the casting and stalled at a 0.4 deg. higher angle of attack than the casting. This simulation caused a slightly sharper drop in C_l post-stall than did the other simulations discussed so far. Despite these minor discrepancies in C_l and stall

behavior, C_d of the simple-geometry simulation agreed extremely well with C_d of the casting. The value of $\Delta C_{d,rms}$ for the simple-geometry simulation was only 7.1%, compared with 23.1% for the 2-D smooth simulation from α = -4 to 9 deg. (again, $\Delta C_{d,rms}$ was calculated using Eq. (1)). However, measurements of C_d at a different station along the airfoil span may have shown worse agreement with the casting C_d. Practical constraints prohibited these spanwise C_d measurements from being taken for every simulation.

Previous studies have shown the aerodynamic performance of an airfoil with a streamwise-ice accretion to be sensitive to roughness height and concentration.[10] Generally, increasing roughness height or concentration caused $C_{l,max}$ to decrease and C_d to increase, similar to what was observed for the ice roughness accretions. In view of these trends, the roughness size on the 2-D smooth simulation was altered in order to match the simulation aerodynamics to the full-scale casting. Since the aerodynamic penalty associated with the 2-D smooth simulation was too severe, it was recognized that the roughness inherently present on the 2-D smooth simulation had to be removed. It is evident in the tracing of the EG1125 streamwise-ice accretion that feathers were present on the accretion and were traced. These feathers are circled in Fig. 10. The 2-D smooth simulation was constructed by extruding this tracing. Therefore, these feathers, which are highly three dimensional in nature, were effectively treated as two-dimensional geometric features in the simulation process, resulting in small, artificial "ridges" along the span of the simulation near the leading edge of the airfoil. To reduce the influence of these ridges, a layer of tape was applied to the 2-D smooth simulation. This effectively smoothed the simulation further and eliminated the ridge caused by the tracing of the feathers. The effect of this tape was to increase $C_{l,max}$ to within 1.1% of the casting $C_{l,max}$ and to prolong stall to α = 11.6 deg. (Fig. 8), nearly the same angle beyond which the casting caused stall. Additionally, C_d decreased to the level of the casting and simple-geometry simulation over a wide range of angle of attack, resulting in a $\Delta C_{d,rms}$ = 8.0%.

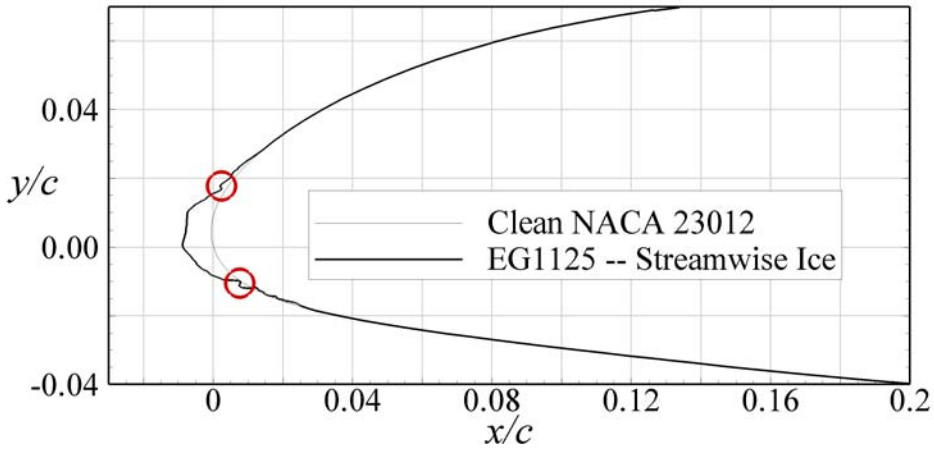

Fig. 10 Location of feathers on ice tracing of EG1125. The feathers were extruded along the entire span of the 2-D smooth simulation, creating a small, artificial "ridge" near the leading edge of the airfoil.

Figure 11 shows the pressure distribution at α = 10 deg. around the NACA 23012 with the full-scale EG1125 casting and two sub-scale simulations. The C_p distribution of the 2-D smooth simulation covered with tape is very similar to the C_p distribution of the casting, which is consistent with the good agreement for C_l and C_d between the two. The 2-D smooth simulation with the roughness scaled to match k/c of the casting had a C_p distribution slightly different from that of the casting. From x/c = 0.02 – 0.10, C_p of this simulation had a lower magnitude than C_p of either the casting or the 2-D smooth simulation covered with tape. Also, C_p at the airfoil trailing edge was greater in magnitude for the 2-D smooth simulation with roughness, suggesting an earlier trailing-edge stall.

The aerodynamic performance data for the full-scale casting and simulations for the EG1162 streamwise-ice accretion, which was more conformal to the airfoil leading edge, are shown in Fig. 12. The 2D-smooth, simple-geometry (Fig. 13), and 2-D smooth + k/c = 0.0013 roughness simulations were all designed with no a priori knowledge of the casting aerodynamics. Of these simulations, the 2-D smooth simulation had $C_{l,max}$ and α_{stall} most similar to the casting, differing by 3.0% and 0.6 deg., respectively. As with the EG1125 streamwise-ice accretion, the simple-geometry simulation had $C_{l,max}$ slightly higher than the casting. The 2-D smooth + k/c = 0.0013 roughness simulation, which directly scaled k/c of the casting, had $C_{l,max}$ 11.7% too low. The penalties to C_d were consistent with these trends in $C_{l,max}$. The 2-D smooth + k/c = 0.0013 roughness simulation had C_d higher than the casting at all angles of attack. Both the simple-geometry and 2-D smooth simulations had C_d similar to the casting

for angles of attack below α = 1 deg. and 3 deg., respectively, but tended to have lower C_d than the casting above these angles. The corresponding values of $\Delta C_{d,rms}$ from α = -4 to 10 deg. were 16.7% and 11.7%.

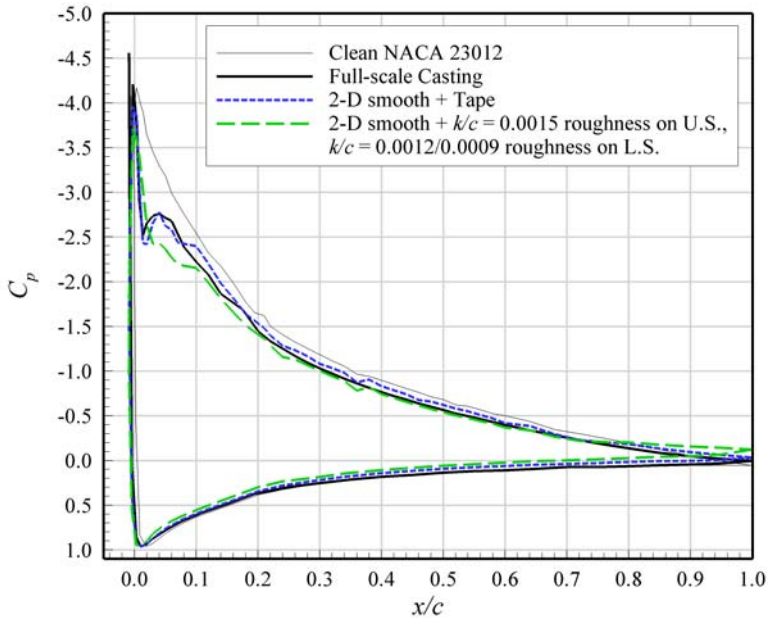

Fig. 11 Pressure distribution around EG1125 streamwise-ice simulations at α = 10 deg.

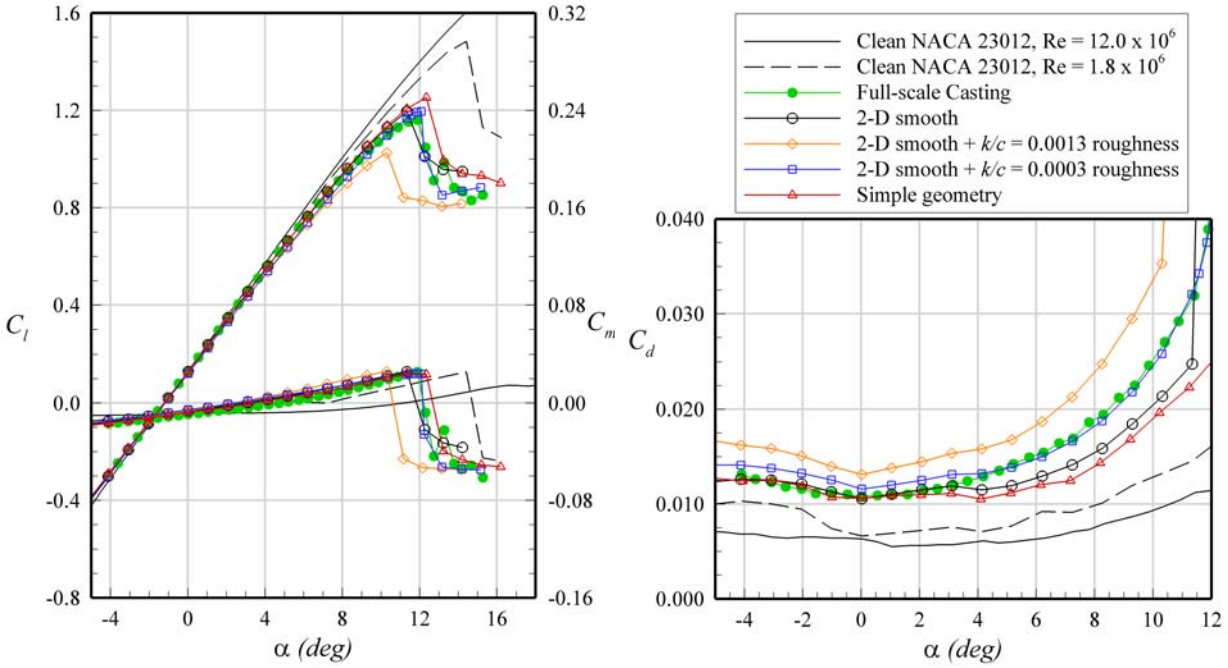

Fig. 12 Comparison of C_l, C_m, and C_d of EG1162 streamwise-ice simulations. The casting data were acquired at Re = 12.0 x 10^6 and M = 0.20, all other data were acquired at Re = 1.8 x 10^6 and M = 0.18.

The 2D-smooth + k/c = 0.0003 roughness simulation was designed *with* a priori knowledge of the casting aerodynamics and resulted from a trade study which varied roughness height on the 2-D smooth simulation. $C_{l,max}$ of this simulation was approximately 3.0% greater than $C_{l,max}$ of the casting, with stall occurring at a 0.2 deg. higher angle. C_d agreed well with the casting, especially with consideration of the uncertainty inherent in measuring C_d at only one spanwise station. The $\Delta C_{d,rms}$ for the 2-D smooth + k/c = 0.0003 roughness was 7.9%. The C_p distributions

for the 2-D smooth simulations with k/c = 0.0003 roughness and with k/c = 0.0013 roughness are compared to the C_p distribution of the EG1162 casting at α = 10 deg. in Fig. 14. The 2-D smooth with k/c = 0.0003 roughness simulation had a C_p distribution almost identical to the C_p distribution of the casting, while the 2-D smooth with k/c = 0.0013 roughness simulation had a trailing-edge pressure that was noticeably higher in magnitude than that of the casting.

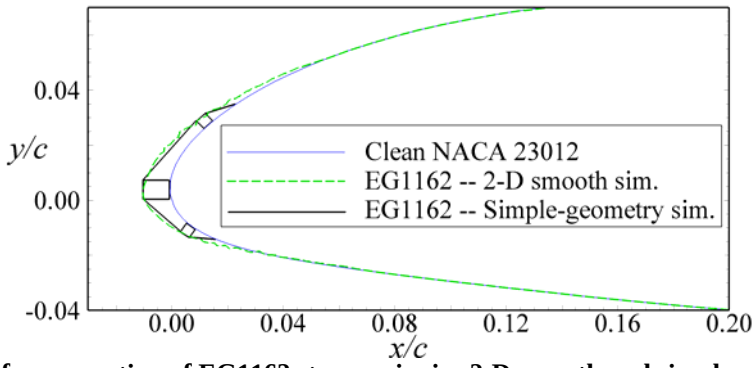

Fig. 13 Comparison of cross-section of EG1162 streamwise ice 2-D smooth and simple-geometry simulations.

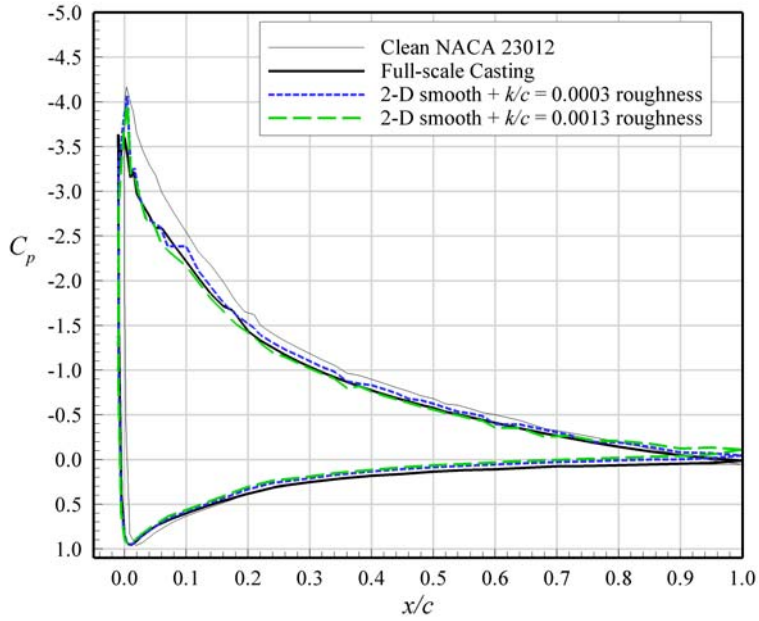

Fig. 14 Pressure distribution around EG1162 streamwise-ice simulations at α = 10 deg.

The results for the simulations of the two streamwise-ice accretions discussed in this section show that modeling surface roughness is important. The 2-D smooth and simple-geometry simulations with no added roughness modeled $C_{l,max}$ and C_d reasonably well, but the aerodynamic fidelity of the 2-D smooth simulations in particular increased considerably when the surface roughness of the simulation was tailored to better match the casting. For the case of the EG1125 streamwise-ice accretion, this required smoothing over the 2-D smooth simulation to eliminate artificially-generated two-dimensional features. For the EG1162 streamwise-ice accretion, it required adding appropriately sized roughness elements to the 2-D smooth simulation.

Horn-ice Simulations

The horn-ice accretion was modeled using sub-scale simple-geometry and 2-D smooth simulations. Tracings of these simulations are shown in Figs. 2 and 15. The horn had a height of k/c = 0.020 and was located at approximately s/c = 0.009. The angle of the horn with respect to the airfoil chord-line was θ = 27 deg. The casting caused a thin-airfoil type stall at α = 8.8 deg., resulting in a $C_{l,max}$ = 0.86 (Fig. 16). It also caused a considerable increase in C_d. Both the sub-scale simulations had similar effects, with the 2-D smooth simulation having a $C_{l,max}$

within 2% of the casting, as shown in Fig. 16. The simple-geometry simulation had a 7% lower $C_{l,max}$. It is possible that this reduced $C_{l,max}$ of the simple-geometry simulation was at least in part due to poor simulation tolerances and positioning inaccuracies, since this simulation was constructed from simple materials rather than rapid-prototyping techniques. The increased $C_{l,max}$ of the casting and 2-D smooth simulations may also have resulted from curvature of the horn, which was not captured with the simple-geometry simulation.

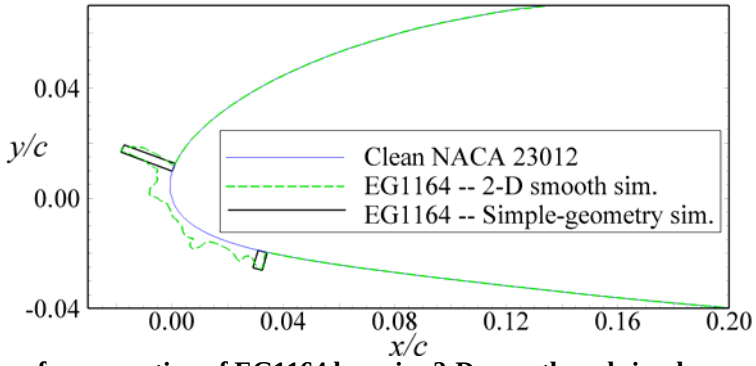

Fig. 15 Comparison of cross-section of EG1164 horn ice 2-D smooth and simple-geometry simulations.

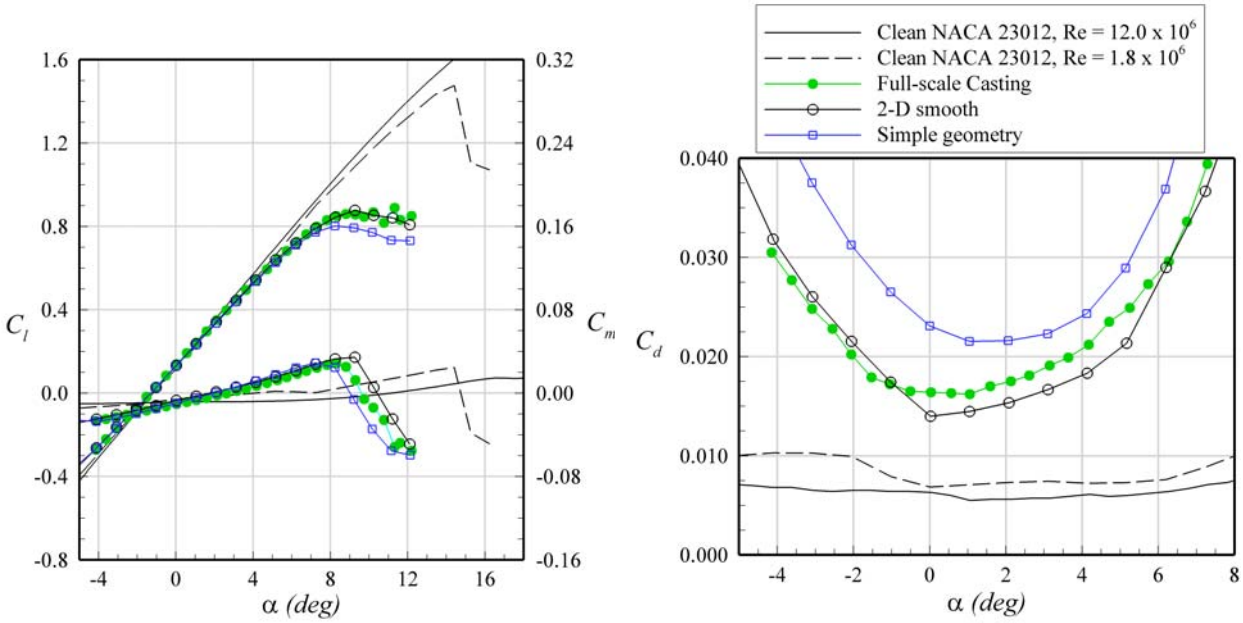

Fig. 16 Comparison of C_l, C_m, and C_d of EG1164 horn-ice simulations. The casting data were acquired at Re = 12.0 x 10^6 and M = 0.20, all other data were acquired at Re = 1.8 x 10^6 and M = 0.18.

Consistent with these results for C_l, the 2-D smooth had a C_d curve similar to that of the casting while the C_d of the simple-geometry simulation was generally higher than that of the casting and much narrower (Fig. 16). The percent RMS difference in C_d for the 2-D smooth simulation from α = -4 to 8 deg. was 10.4%, while it was nearly 37% for the simple-geometry simulation. These results for $C_{l,max}$ compare reasonably well to the earlier study by Busch[8] comparing sub-scale 2-D smooth and simple-geometry simulations to a sub-scale horn-ice accretion casting, suggesting, at least for horn-ice, that geometric scaling (maintaining a constant horn k/c) is appropriate and that Reynolds number does not need to be matched to obtain an accurate estimate of iced-airfoil performance.

The pressure distributions around the horn-ice casting and each of the simulations at α = 8 deg. are shown in Fig. 17. The severe adverse pressure gradient at the tip of the horn causes a rapid acceleration of the flow around the tip followed by flow separation, resulting in a separation bubble. The pressure distribution of the casting in Fig. 17 captured both of these effects. The pressure tap on the casting at the tip of the horn measured a highly localized region of low pressure at x/c = -0.018, with a C_p = -2.62. Downstream of this chordwise station is a region of approximately constant pressure extending to x/c = 0.050, with $C_p \approx$ -2.35, indicating the presence of a separation

bubble. Farther downstream of this point, pressure recovery begins inside the bubble. The relative qualitative sizes of the separation bubbles generated by each of the horn simulations can be estimated from the pressure distribution. The larger negative C_p in the separation bubble of the 2-D smooth simulation and the more upstream *x/c* location where pressure recovery begins indicates that the 2-D smooth simulation has a smaller separation bubble than does the casting. Along those lines, the lower magnitude constant C_p and larger chordwise extent of the constant-pressure region in the pressure distribution of the simple-geometry simulation indicates that it has a larger separation bubble than the casting. These trends are consistent with the results for $C_{l,max}$ and C_d, as ice simulation geometries which generate larger separation bubbles have been shown to cause larger aerodynamic penalties than those which generate smaller separation bubbles.[5] Note that the simple-geometry simulation used the clean airfoil pressure taps. No additional pressure taps were installed on the horn itself, so there was no measured C_p corresponding to pressure on the horn for this simulation.

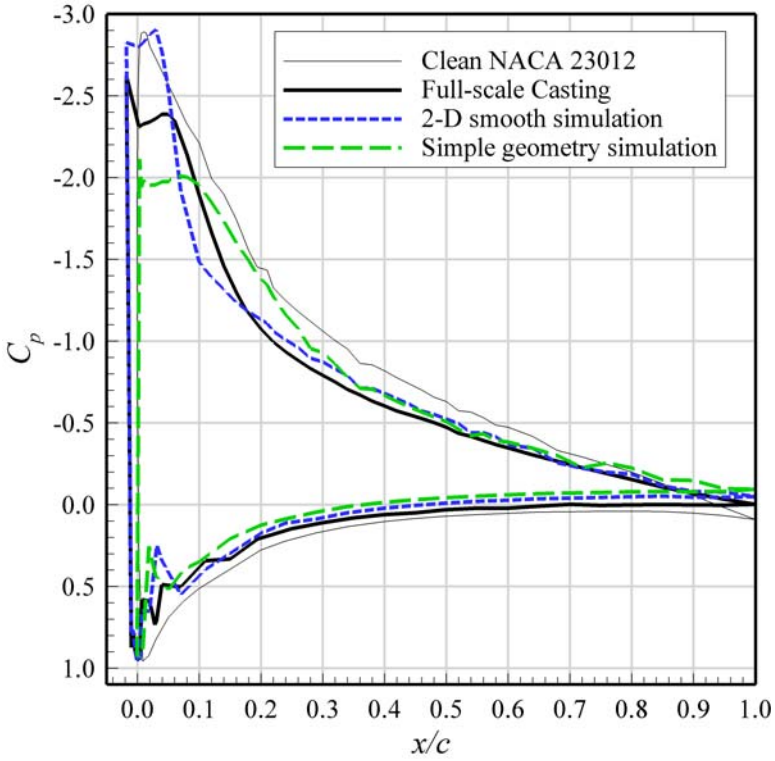

Fig. 17 Pressure distribution around EG1164 horn-ice simulations at α = 8 deg.

Spanwise-ridge Ice Simulations

As discussed in the Introduction, spanwise-ridge ice often results from the use of a thermal ice protection system (IPS) on the leading-edge. The spanwise-ridge ice accretion (EG1159) in this study was generated using a simulated thermal IPS, so the leading edge of the airfoil remained free of ice. However, a spanwise ridge formed downstream of the IPS, at *x/c* = 0.05 on the upper surface. This ridge had a height *k/c* = 0.013 and an angle of θ = 67 deg. with respect to the airfoil chord-line. On the lower surface, a smaller ridge formed downstream of the IPS. This ridge was more three-dimensional than the upper surface ridge and had a height at the tracing location of *k/c* = 0.0052.

C_l, C_m, and C_d for the EG1159 spanwise-ridge casting are shown in Fig. 18. The ridge casting caused a more severe penalty in aerodynamic performance than did any of the other simulations, causing stall to occur at a much lower α = 5.1 deg. This stall was much more gradual than the stall for the clean NACA 23012. $C_{l,max}$ was reduced to 0.48. Additionally, $C_{d,min}$ increased to about 0.0226 and occurred near α = -4 deg. These values correspond to a 74% decrease in $C_{l,max}$ and a 311% increase in $C_{d,min}$ compared to the clean NACA 23012 airfoil at $Re = 12.0 \times 10^6$.

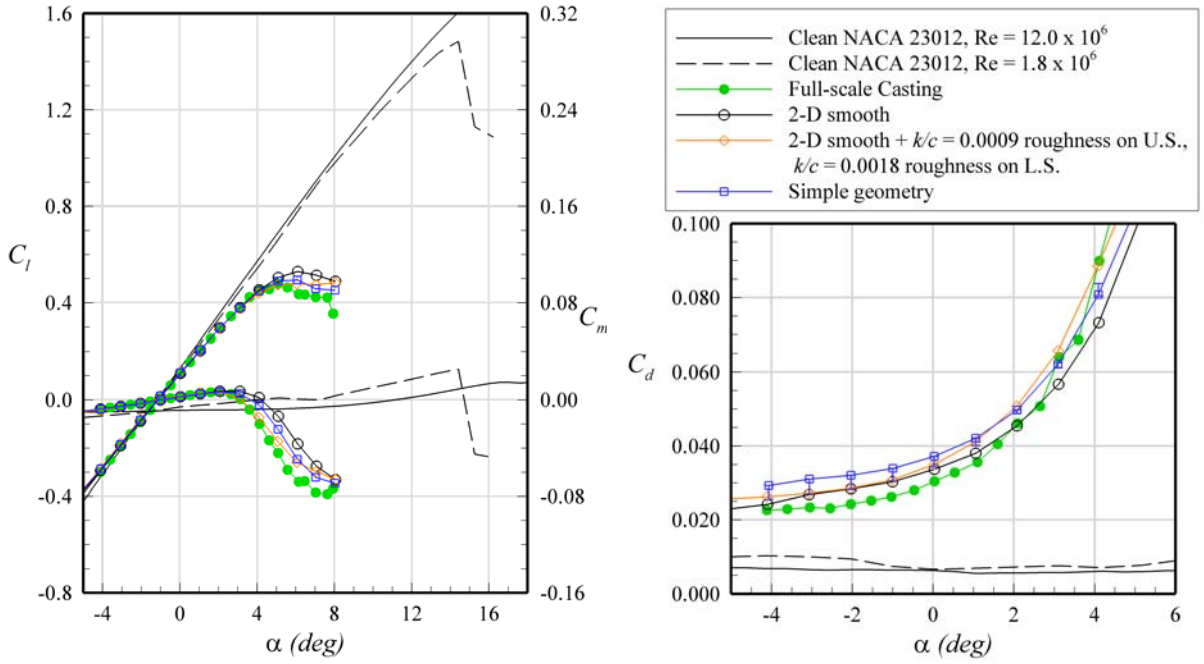

Fig. 18 Comparison of C_l, C_m, and C_d of EG1159 spanwise-ridge ice simulations. The casting data were acquired at Re = 12.0 x 10^6 and M = 0.20, all other data were acquired at Re = 1.8 x 10^6 and M = 0.18. The error bars indicate the variation in C_d along the airfoil span.

Simple-geometry and 2-D smooth simulations (shown in Fig. 19) with and without roughness were designed to model the aerodynamic performance of the spanwise-ridge ice accretion, and the performance of these simulations are compared to that of the casting in Fig. 18. The 2-D smooth simulation had $C_{l,max}$ higher than the casting by about 10.6 % and stalled at a 1.0 deg. higher angle of attack. However, it did a reasonable job of modeling C_d, having a $\Delta C_{d,rms}$ = 12.8%. Roughness with height k/c = 0.0009 and k/c = 0.0018 was added to the upper and lower surface of the 2-D smooth simulation, respectively, to match the k/c and extents of the roughness on the spanwise-ridge casting (x/c = 0.048 to 0.068 on the upper surface, x/c = 0.095 to 0.14 on the lower surface). This caused a slight reduction in $C_{l,max}$, giving a value within 1.0% of the casting. This simulation had a stall that was even more gradual than the stall of the casting, with C_l leveling off but not decreasing over the range of angle of attack at which C_l was measured. The addition of roughness caused an increase in C_d at positive angles of attack. This worsened the comparison with the casting from α = 0 to 2 deg., but improved agreement above α = 2 deg. Over the range α = -4 to 4 deg., $\Delta C_{d,rms}$ increased slightly to 13.9%.

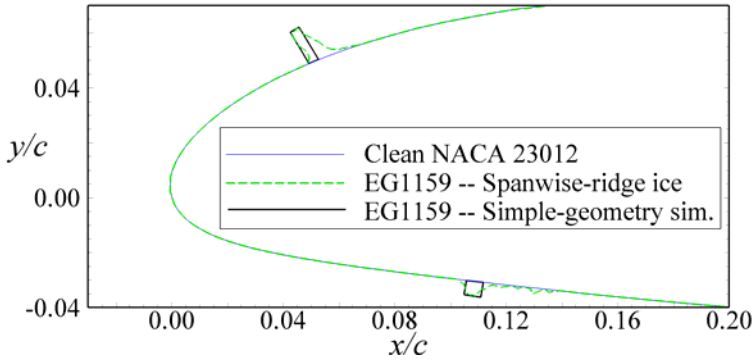

Fig. 19 Comparison of cross-section of EG1159 spanwise-ridge ice 2-D smooth and simple-geometry simulations.

The aerodynamic performance of a simple-geometry simulation of the ridge is also shown in Fig. 18. $C_{l,max}$ of this simulation was about 3.3% higher than that of the casting and slightly below $C_{l,max}$ of the 2-D smooth

simulation. Like the 2-D smooth simulation, the simple-geometry simulation had C_d slightly too high at low angle of attack and slightly too low at very high angle of attack. To gauge the variation in C_d along the span of the airfoil, C_d measurements were taken at 5 different spanwise stations two inches apart behind the simple-geometry simulation (a nominally two-dimensional simulation). The error bars shown in Fig. 18 (associated with the simple-geometry simulation) are representative of the minimum and maximum C_d values obtained in this spanwise sweep. At negative angles of attack, the variation in C_d along the airfoil span is on the order of 10%. At positive angles of attack, the variation is on the order of 3%. It is likely that similar variations were present on the 2-D smooth simulations and on the casting during the F1 testing. With this consideration, C_d of the 2-D smooth simulation with added roughness is very similar to C_d of the casting below $\alpha = 2$ deg. Above $\alpha = 2$ deg., the C_d of the 2-D smooth simulation is below that of the casting, independent of the spanwise station at which C_d was measured.

The pressure distribution around the spanwise-ridge ice casting is shown in Fig. 20. The ridge eliminates the suction peak on the leading-edge region of the airfoil. At $x/c = 0.05$, the location of the upper surface ridge, the pressure decreases suddenly. Similar to the horn-ice accretion, the pressure tap located at the tip of the ridge captures the rapid acceleration of flow over the ridge tip, resulting in a small spike in the C_p distribution at $x/c = 0.05$. As with the horn-ice accretion, the severe adverse pressure gradient at the tip of the ridge causes flow separation downstream of the ridge, resulting in a separation bubble. This is indicated by the region of constant pressure extending downstream of $x/c = 0.05$ to $x/c = 0.20$ (for the casting). The C_p distribution also shows a reduced pressure recovery relative to the clean airfoil case, resulting in lower trailing-edge pressure on the iced airfoil.

Qualitatively, the C_p distributions of the sub-scale spanwise-ridge ice simulations look very similar to the C_p distribution of the full-scale casting (Fig. 20). Like the casting, the sub-scale simulations eliminate the leading-edge suction peak, generate separation bubbles, and reduce pressure recovery. However, the separation bubbles downstream of the ridge appear to be slightly smaller for the sub-scale simulations than for the casting. The constant pressure region extends only to about $x/c = 0.15$ for the 2-D smooth simulation and $x/c = 0.18$ for the simple-geometry simulation and 2-D smooth simulation with roughness. Also indicative of smaller separation bubbles on the sub-scale simulations is the higher magnitude of the constant pressure plateau, which ranges from about $C_p \approx -1.30$ to -1.44 for the sub-scale simulations compared with $C_p \approx -1.18$ for the casting. The C_p distributions for the casting and 2-D smooth simulations with and without roughness look similar on the lower surface also. The C_p distribution of the simple-geometry simulation does not appear to capture the separation bubble behind the lower surface ridge as well as the 2-D smooth simulations because it had no pressure taps in that location.

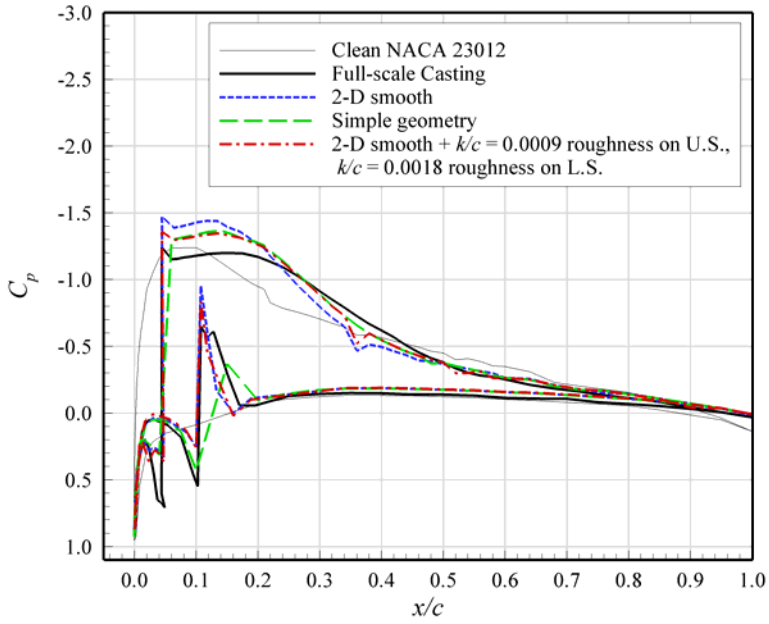

Fig. 20 Pressure distribution around EG1159 spanwise-ridge ice simulations at $\alpha = 3$ deg.

To further compare the flowfields of the casting and sub-scale simulations, surface oil-flow visualization images were acquired. Figure 21(a) is an oil-flow visualization image of the full-scale casting taken at $\alpha = 3$ deg. at

Re = 12.0 x 10^6 and M = 0.20. Flow is from left to right, and the spanwise-ridge casting is visible on the far left of the image. The estimated mean separation bubble reattachment location has been highlighted, and is positioned at approximately x/c = 0.44. Downstream of this line, the flow moves toward the airfoil trailing edge. Upstream of this line is a region of recirculation inside the separation bubble generated by the ridge. Flow on the airfoil surface in this region is in the upstream direction, toward the airfoil leading edge. Figure 21(b) is an oil-flow visualization image of the spanwise-ridge ice 2-D smooth simulation at α = 3 deg. In this figure, the pressure tap row (used to obtain the C_p distribution) is located at the z = 0-inch spanwise station. Like the C_p distribution, the flowfield around the 2-D smooth simulation is qualitatively similar to that of the casting. Again, the estimated separation bubble mean reattachment location has been highlighted, with recirculating flow upstream of this region and flow toward the airfoil trailing edge downstream of this region. For this simulation, reattachment is estimated to have occurred at x/c = 0.33. This smaller separation bubble on the 2-D smooth simulation is consistent with the C_p distribution of Fig. 16. Note that there is slightly more spanwise non-uniformity in the flowfield of the 2-D smooth simulation than in the flowfield of the casting, but overall both flowfields appear to be reasonably two-dimensional at this angle of attack.

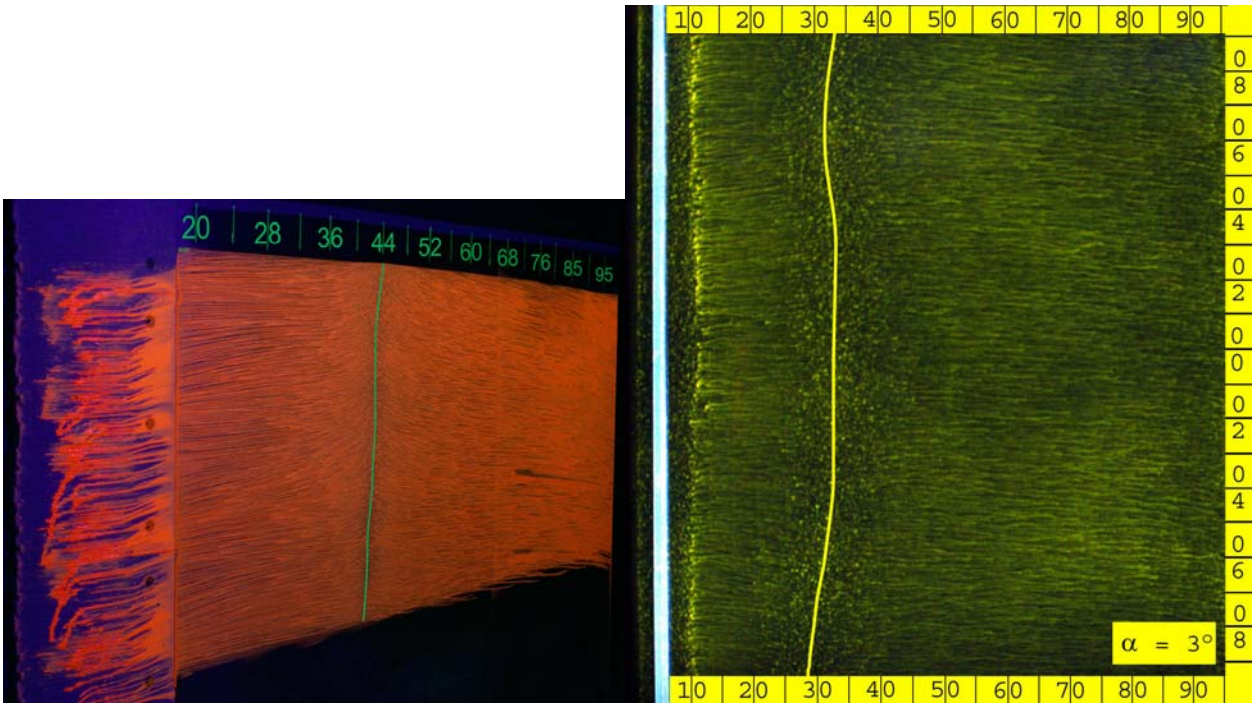

(a) **(b)**

Fig. 21 Surface oil-flow visualization images of EG1159 spanwise-ridge ice simulations on NACA 23012 airfoil at α = 3 deg.: (a) Full-scale casting at Re = 7.8 x 10^6 and M = 0.20 and (b) sub-scale 2-D smooth simulation at Re = 1.8 x 10^6 and M = 0.18. Flow is from left to right. The estimated mean separation bubble reattachment location has been highlighted in each case.

IV. Summary and Conclusions

The objective of this study was to quantify the accuracy with which sub-scale, two-dimensional ice accretion simulations at low Reynolds number can represent the aerodynamic performance of full-scale ice accretion castings at high Reynolds number. Tracings of six full-scale castings from each of four categories of ice accretion were digitized and measured. From these measurements, ¼-scale 2-D smooth and simple geometry simulations with and without surface roughness were constructed and installed on an 18-inch chord NACA 23012. C_l, C_m, and C_d were measured in the University of Illinois 3 x 4 ft. subsonic wind tunnel at Re = 1.8 x 10^6 and M = 0.18. These data were compared to aerodynamic performance data for the corresponding full-scale castings on a 72-inch chord NACA 23012 airfoil. These data had already been acquired in the ONERA F1 wind tunnel at Re = 12.0 x 10^6 and M = 0.2. Results were presented for geometrically-scaled simulations, with roughness height k/c similar to that of the full-scale casting, and also for simulations which were designed based on a priori knowledge of the casting aerodynamics.

A summary of the aerodynamic fidelity of the geometrically-scaled simulations for the clean airfoil and each casting is given in Table 1. This table summarizes the simulations that were based solely on the geometry of the casting and required no a priori knowledge of the casting aerodynamics. Data for the clean NACA 23012 is also provided to show the effect of Reynolds number on the clean airfoil performance. When examining these comparisons, it is important to note that the differences between most simulations of a given ice accretion are small compared to the original degradation in aerodynamic performance from the clean airfoil.

For all ice accretion types, geometric scaling resulted in conservative estimates of $C_{l,max}$. For horn and spanwise-ridge ice accretions, the geometrically-scaled simulations had $C_{l,max}$ within 2% of the castings. For ice roughness and streamwise-ice accretions, the geometrically-scaled simulations generally had significantly lower $C_{l,max}$ than the castings. The last column in Table 1 quantifies the agreement between C_d of a simulation and C_d of the corresponding casting. As with the modeling of $C_{l,max}$, the horn and spanwise-ridge ice accretion simulations tended to have better agreement with the casting than did the ice roughness and streamwise-ice simulations.

Table 2 provides a summary of the simple-geometry and 2-D smooth simulations that had aerodynamic performance most similar to the corresponding castings. These simulations were built after the geometrically-scaled simulations had already been tested and were designed to provide improved agreement with the casting. Generally, this required that a smaller roughness size be used, with *k/c* of the simulation less than *k/c* of the casting. As would be expected, agreement in both $C_{l,max}$ and C_d improved substantially for most accretion types. $C_{l,max}$ was modeled to within 3% and $\Delta C_{d,rms}$ was less than 12% for all accretion types.

Table 1 Summary of aerodynamic fidelity of geometrically-scaled two-dimensional ice casting simulations. These simulations were designed with no a priori knowledge of the casting aerodynamics.

Accretion Type	Geometrically Scaled Simulation	Simulation $C_{l,max}$ - Casting $C_{l,max}$	Simulation α_{stall} - Casting α_{stall} (deg)	Δ RMS C_d Simulation v. Casting (Linear α Range)
72" chord NACA 23012, Re = 12.0 million	18" chord NACA 23012, Re = 1.8 million	-0.352 (-23.7%)	-3.7	36.0%
Glaze Ice Roughness, EG1126	Simple geometry + *k/c* = 0.0013/0.0005 roughness on U.S., *k/c* = 0.0009/0.0003 roughness on L.S.	-0.042 (-3.9%)	-1.1	20.3%
Rime Ice Roughness, EG1134	Simple-geometry + k/c = 0.0003 roughness (EG1126 extents)	-0.200 (-15.7%)	-1.6	29.50%
Streamwise Ice, EG1125	2-D smooth + *k/c* = 0.0015 roughness on U.S., *k/c* = 0.0012/0.0009 roughness on L.S.	-0.120 (-10.6%)	-0.6	47.6%
Streamwise Ice, EG1162	2-D smooth + k/c = 0.0013 roughness	-0.135 (-11.7%)	-1.6	26.0%
Horn Ice, EG1164	2-D smooth	-0.016 (-1.9%)	0.0	10.4%
Spanwise-ridge Ice, EG1159	2-D smooth + *k/c* = 0.0009 roughness on U.S., *k/c* = 0.0018 roughness on L.S.	-0.005 (-1.0%)	2.0	13.9%

Conclusions

1. For ice roughness and streamwise-ice accretions, modeling the height and concentration of surface roughness is important. The chordwise extents of the roughness do not have a noticeable effect on $C_{l,max}$, but do on C_d.

2. Geometric scaling of roughness height on ice roughness and streamwise-ice simulations tended to cause unrepresentatively large penalties to $C_{l,max}$ and C_d when the roughness was applied at a high concentration. Reducing roughness concentration would help decrease these penalties, but at this time, no accurate method for measuring roughness concentration on an ice accretion has been developed.

3. When using an ice tracing to generate a 2-D smooth simulation, highly three-dimensional features, such as ice feathers, should be smoothed out. Extruding such a feature along the airfoil span will result in an artificial, two-dimensional feature which may not have the proper effect on $C_{l,max}$ and C_d.

4. For horn-ice accretions, accurately representing the height, angle, and location of the horn using a 2-D smooth simulation provided an accurate representation of $C_{l,max}$

5. When possible, C_d measurements should be taken at several stations along the airfoil span when making C_d comparisons.

Table 2 Summary of aerodynamic fidelity of most accurate ice casting simulations. These simulations required a priori knowledge of the casting aerodynamics. For the horn-ice accretion, the geometrically-scaled simulation was the most accurate simulation.

Accretion Type	Most Accurate Simulation	Simulation $C_{l,max}$ - Casting $C_{l,max}$	Simulation α_{stall} - Casting α_{stall} (deg)	Δ RMS C_d Simulation v. Casting (Linear α Range)
Glaze Ice Roughness, EG1126	Simple-geometry + s/c = 0.0055 strips of k/c = 0.0013 roughness on U.S., k/c = 0.0009 roughness on L.S.	-0.03 (-2.8%)	-1.1	11.4%
Rime Ice Roughness, EG1134	Simple-geometry + k/c = 0.00007 roughness	0.008 (0.6%)	0.0	6.84%
Streamwise Ice, EG1125	2-D smooth, covered with tape	-0.009 (-0.8%)	-0.3	8.0%
Streamwise Ice, EG1162	2-D smooth + k/c = 0.0003 roughness	0.034 (3.0%)	0.2	7.9%
Spanwise-ridge Ice, EG1159	2-D smooth + k/c = 0.0003 roughness	-0.01 (-1.4%)	1.9	10.0%

Acknowledgments

This research was supported by NASA grants NCC3-1039 and ASRC, Inc. subcontract AS3304 from the NASA Glenn Research Center. The authors wish to thank Gene Addy from NASA Glenn and Sam Lee from ASRC Aerospace Corp. for their helpful advice during this investigation. Thanks also go to Austin Ellis at the University of Illinois for his assistance in the data reduction portion of this study.

References

[1] Bragg, M., Broeren, A., Addy, H., Potapczuk, M., Guffond, D., and Montreuil, E., "Airfoil Ice-Accretion Aerodynamic Simulation," AIAA-2007-0085, *45th Aerospace Sciences Meeting & Exhibit*, Reno, NV, Jan. 2007.

[2] Vickerman, M.B., Choo, Y.K., Schilling, H.W., Baez, M., Braun, D.C., and Cotton, B.J., "Toward an Efficient Icing CFD Process Using an Interactive Software Toolkit – SmaggIce 2D," AIAA-2002-0380, *40th Aerospace Sciences Meeting & Exhibit,* Reno, NV, Jan 2002.

[3] Papadakis, M., Alansatan, S., and Seltmann, M. "Experimental Study of Simulated Ice Shapes on a NACA 0011 Airfoil," AIAA-1999-0096, *37th AIAA Aerospace Sciences Meeting & Exhibit*, Reno, NV, Jan. 1999

[4] Kim, H., "Effects of Leading-edge Ice Accretion Geometry on Airfoil Performance," M.S. Thesis, Dept. of Aerospace Engineering, Univ. of Illinois, Urbana, IL, 2004.

[5] Bragg, M. B., Broeren, A. P., and Blumenthal, L. A., "Iced-Airfoil Aerodynamics," *Progress in Aerospace Sciences*, Vol. 41, 2005, pp. 323-362.

[6] Tani, I., "Low Speed Flows Involving Bubble Separations," *Progress in Aerospace Sciences*, Vol. 5, 1964, pp. 70–103.

[7] McCullough, G.B., and Gault, D.E., "Examples of Three Representative Types of Airfoil-Section Stall at Low Speed," NACA TN-2502, Sep. 1951.

[8] Busch, G. T., "Ice Accretion Aerodynamic Simulation on a Sub-scale Model," M.S. Thesis, Univ. of Illinois, Urbana, IL, 2006.

[9] Busch, G.T., Broeren, A.P., and Bragg, M.B., "Aerodynamic Simulation of a Horn-ice Accretion on a Sub-scale Model," AIAA-2007-0087, *45th AIAA Aerospace Sciences Meeting & Exhibit*, Reno, NV, Jan. 2007.

[10] Broeren, A.P., Busch, G.T., and Bragg, M.B., "Aerodynamic Fidelity of Ice Accretion Simulation on a Sub-scale Model," SAE Paper 2007-01-3285, 2007.

[11] Broeren, A.P. Bragg, M.B., Addy, Jr., H.E., Lee, S., Moens, F., and Guffond, D., "Effect of High-Fidelity Ice Accretion Simulations on the Performance of a Full-Scale Airfoil Model," AIAA-2008-0434, *46th Aerospace Sciences Meeting & Exhibit*, Reno, NV, Jan. 2008.

[12] Addy, Jr., H. E. and Chung, J. J., "A Wind Tunnel Study of Icing Effects on a Natural Laminar Flow Airfoil," AIAA–2000–0095, *38th AIAA Aerospace Sciences Meeting & Exhibit*, Reno, NV, Jan. 2000.

[13] Papadakis, M., Gile Laflin, B. E., Youssef, G. M., and Ratvasky, T. P., "Aerodynamic Scaling Experiments with Simulated Ice Accretions," AIAA-2001-0833, *39th AIAA Aerospace Sciences Meeting & Exhibit*, Reno, NV, Jan. 2001.

[14] Lee, S., Kim, H.S., and Bragg, M.B., "Investigation of Factors that Influence Iced-Airfoil Aerodynamics," AIAA-2000-0099, *38th Aerospace Sciences Meeting & Exhibit*, Reno, NV, Jan. 2000.

[15] Broeren, A.P., "An Experimental Study of Unsteady Flow over Airfoils near Stall," Ph.D. Dissertation, Univ. of Illinois, Urbana, IL, 2000.

[16] Blumenthal, L., "Surface Pressure Measurement on a Three-Dimensional Ice Shape," M.S. thesis, University of Illinois at Urbana-Champaign, 2005.

[17] Busch, G.T., Broeren, A.P., and Bragg, M.B., "Aerodynamic Simulation of a Horn-ice Accretion on a Subscale Model," AIAA-2007-0087, *45th Aerospace Sciences Meeting & Exhibit,* Reno, NV, Jan. 2007.

[18] Jackson, D.G., "Effect of Simulated Ice and Residual Ice Roughness on the Performance of a Natural Laminar Flow Airfoil," M.S. Thesis, Univ. of Illinois, Urbana, IL, 1999.